INTERNATIONAL JOURNAL FOR NUMERICAL METHODS IN FLUIDS, VOL. 19, 153–176 (1994)

SIMULATION OF IMPACTS OF FLUID FREE SURFACES WITH SOLID BOUNDARIES

DAVID B. JOHNSON, PETER E. RAAD AND SHEA CHEN

Mechanical Engineering Department, Southern Methodist University, Dallas, Texas 75275-0335, U.S.A.

SUMMARY

Deficiencies associated with the simulation of impacts of fluid free surfaces with solid boundaries by use of marker-and-cell methods are identified and addressed. New procedures are introduced that affect the movement of markers in cells adjacent to a solid boundary, the flags of the cells that comprise a solid boundary and the pressure boundary condition for a cell in which impact occurs. Combined with fundamental changes in the sequence of steps in the computational cycle, these new procedures allow the *intentional* treatment of impact. As a result, improved estimates are obtained of the pressure associated with the cells adjacent to a boundary along which impact occurs. Consequently, more appropriate adjustments are made of the tentative internal velocities associated with such cells. In addition, a special procedure is presented for the adjustment of the tentative internal velocity between two surface cells. Finally, a new cell type termed a corner cell is defined and a procedure for its treatment is presented. Numerical examples are included to illustrate the previous deficiencies associated with the simulation of impact as well as the effectiveness of the new methods presented in this paper. Validation of the new methods is achieved by comparison with experimental results for spillage over a containment dike.

KEY WORDS Free surface fluid flow Impact Viscous Incompressible Two-dimensional Finite difference simulation Marker and cell

1. INTRODUCTION

Free surface fluid flow occurs in a wide variety of situations ranging from ocean waves running up on a beach to cavity filling in a casting or moulding process in manufacturing. A distinguishing feature of these fluid flows that complicates the development of a numerical simulation technique is the existence of free surfaces that continuously change shapes and locations.

In 1965 Harlow and Welch[1] and Welch *et al.*[2] presented the marker-and-cell (MAC) method, a free surface fluid flow simulation method that introduced the use of massless markers that move with the fluid and a novel solution algorithm for the velocity field. Since 1965 a number of authors have presented extensions and modifications of the original marker-and-cell method. In 1967 Chorin[3] presented a method for calculating steady state solutions of the equations of motion of an incompressible fluid. Chorin introduced the use of an artificial density and sought a steady state solution for which the rates of change of this artificial density and of the velocities all vanished. He thereby avoided the necessity of solving the pressure Poisson equation presented in the MAC method. In 1969 Viecelli[4] adapted Chorin's method of solving simultaneously for the pressure and velocity fields into the MAC scheme of tracking the free surface of a fluid with markers. In his paper Viecelli also presented a technique for dealing with arbitrarily shaped external boundaries. The simplified marker-and-cell (SMAC) method presented in 1970 by Amsden and Harlow[5] was a significant revision of the MAC method and has been widely

CCC 0271–2091/94/140153–24

Received 18 November 1992
Revised 29 November 1993

referenced. In SMAC Amsden and Harlow present an alternative pressure potential Poisson equation and a scheme for applying the normal stress condition on the free surface of the fluid. By avoiding the need in the MAC method for second-order derivatives of the velocity on the boundary, they significantly simplified the calculation of the pressure potential field that is used to compute the velocity field. In 1971 Viecelli[6] showed the equivalence between his approach to simultaneously advance the pressure and velocity fields and the two-stage approach used in the marker-and-cell method. In 1972 Hirt and Cook[7] noted Viecelli's conclusion that the two-stage approach of the marker-and-cell method and the simultaneous approach to the solution of the pressure and velocity fields are equivalent. In their paper they opted to use the simultaneous procedure for the reason that its use simplifies the application of boundary conditions. In 1975 Hirt *et al.*[8] used the simultaneous approach in an extension of the original MAC method (which they called SOLA) that made use of upwinding in order to control the temporal stability of the solution. In 1980 Nichols *et al.*[9] presented a new method for tracking the free surface of the fluid that used a volume-of-fluid function instead of the markers used in the marker-and-cell method. Their method, called SOLA-VOF, was similar to SOLA in all other respects. In 1987 Gresho and Sani[10] presented a detailed discussion of pressure boundary conditions in the context of numerical solutions of the incompressible Navier–Stokes equations for bounded flow. They stressed the importance of using consistent pressure Poisson equations and boundary conditions. They demonstrated that, given an initially divergence-free fluid flow field, the use of Neumann pressure boundary conditions ensured the continued satisfaction of the divergence-free condition. In 1991 Rosenfeld *et al.*[11] presented a method for solving unsteady, incompressible, bounded fluid flow problems in general curvilinear co-ordinates. They used an implicit temporal fractional step method, except for the diffusion terms which they handled explicitly. Their basic calculational cycle followed that of the marker-and-cell method, including the use of a pressure Poisson equation which they solved by the use of a multigrid scheme. Also in 1991 Chen *et al.*[12] presented the surface marker (SM) method, which incorporated new marker movement and cell-reflagging techniques into the SMAC method and resulted in significant reductions in computer time and memory requirements when tracking the free surface of a fluid in a transient flow problem.

The focus of this paper is on the simulation of the impacts of fluid free surfaces with solid boundaries by use of a marker-and-cell method. Such impacts are not uncommon. They occur, for example, when a wave running up a beach reaches a solid obstacle or when a fluid filling a cavity reaches a solid boundary of the cavity. Few experimental results for such flows have been presented in the literature. In 1978 Greenspan and Young[13] published the results of an experimental investigation into the overflowing of a containment dike subsequent to the total collapse of a fluid reservoir. Various dike configurations were considered, with special attention given to the percentage of fluid clearing the dike as a result of the fluid's dynamic impact with the dike. In 1988 Dear and Field[14] presented photographs depicting the impact of a rectangular solid with a gelatin sheet held between glass blocks. They were able to record the existence and propagation of pressure waves within the gelatin as well as the formation and ejection of liquid jets from the sides of the impact area after the region of liquefaction of the gelatin due to the passage of the high-pressure waves through the gelatin reached the outside edges of the area of impact between the solid projectile and the gelatin. Their experiment does not, however, represent a case of a free surface of a Newtonian fluid impacting a solid obstacle, whereas the experiment of Greenspan and Young represents just such a case. In Section 7 the results of Greenspan and Young are used to validate the overall numerical method presented in this paper and, consequently, the specific procedures introduced to deal with fluid impact with solid obstacles. To facilitate the discussion of procedures used in previous methods as well as the

presentation of new procedures for the simulation of impact, it is necessary to describe some of the fundamental details of the computational method.

We choose the SMAC two-stage computational cycle as the point of departure for the following reasons. (i) It has been argued by many, including Viecelli, Hirt, Nichols, Rosenfeld and their co-workers, that the fundamental calculational approaches employed by MAC, Chorin, Viecelli and SMAC are essentially equivalent. (ii) One main disadvantage of the SMAC two-stage computational cycle lies in its requirement to solve an auxiliary Poisson equation for the pressure potential, which is inefficient as compared with a simultaneous pressure–velocity iterative approach. This point has been addressed by the authors' use of a preconditioned conjugate gradient method, which not only has greatly improved the efficiency of the solution of the Poisson equation but also has eliminated the sticky issue of solvability associated with the previously used successive overrelaxation method. (iii) Another disadvantage of the use of the marker-and-cell method is the considerable computational time and memory required to manage the markers. This point has been addressed by the development of the surface marker method. (iv) The SMAC code is readily available directly from the 1970 Los Alamos Report LA-4370.

It is important to note that (i) the treatment of the approach of the fluid towards a solid obstacle, (ii) the details of the treatment of the impact of the fluid with the obstacle and (iii) the details of the treatment of the cells in the neighbourhood of the impact *all* are important for *any* simulation of free surface fluid flow involving impact. The conceptual contributions made in this paper in connection with these important points are applicable in general to any simulation method for free surface fluid flow, whether pressure and velocity are solved for in two stages or simultaneously. Although the details of the incorporation of the contributions are provided for a simulation method in which the pressure and velocity are solved for in two stages, it is equally important to intentionally treat impact in a simulation method in which a simultaneous approach is used and the same considerations are necessary in connection with such a method.

In marker-and-cell methods the computational region is divided into rectangular cells and the staggered grid concept is employed to locate the discrete field variables. For cell (i, j) shown in Figure 1, the velocities $u_{i,j}$, $v_{i,j}$, $u_{i-1,j}$, and $v_{i,j-1}$ are located at the midpoints of the faces of the cell, while the pressure potential* $\psi_{i,j}$ is located at the centre of the cell. Each cell within the computational domain is flagged at each discrete value of time as one of four types: EMP, SUR, FUL or OB. EMP represents a cell that has no fluid in it; SUR represents a cell that contains fluid and is adjacent to an EMP cell; FUL represents a cell that contains fluid and has no EMP neighbours; and OB represents a cell that defines the location of a solid, stationary

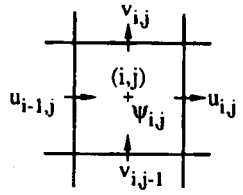

Figure 1. Staggered grid locations of field variables for cell (i, j)

* The pressure potential rather than the pressure is calculated in the SMAC method.[5] The Poisson equation for the pressure potential is presented in Figures 4 and 5. Gradients of the pressure potential are employed to correct the tentative velocities for the effect of pressure by use of equations that also are presented in Figures 4 and 5.

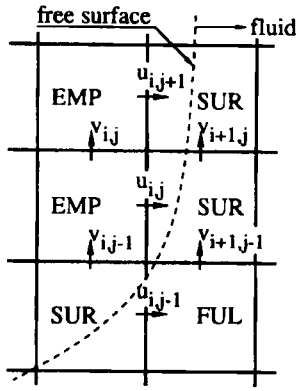

Figure 2. Examples of internal, surface and just outside tangential velocities

obstacle. A velocity on a face shared by any combination of SUR and FUL cells is referred to as an internal velocity; a velocity that is normal to a face shared by an SUR cell and an EMP cell is referred to as a surface velocity; and a velocity on a face between two EMP cells which in turn are adjacent to SUR cells is termed a just outside tangential velocity. Surface velocities and just outside tangential velocities represent free surface velocity boundary conditions. Examples of the three types of velocities are shown in Figure 2, where $v_{i+1,j-1}$ and $v_{i+1,j}$ are internal velocities, $v_{i,j-1}$, $u_{i,j}$, and $u_{i,j+1}$ are surface velocities and $v_{i,j}$ is a just outside tangential velocity. The treatment of free surface pressure and velocity boundary conditions has a determining influence on the simulation of free surface fluid flow. The treatment of free surface boundary conditions is not, however, the focus of this paper. The focus instead is on all aspects of the treatment of the impact of a fluid free surface with a solid obstacle.

It is important to note, however, that although the two-stage SMAC computational cycle serves as the point of departure for the new treatment of impact, the new simulation method presented in this paper incorporates velocity boundary conditions that are different from those used in SMAC. For example, although our rationale is different, the just outside tangential velocity scheme used is the one introduced by the original MAC method. If any other scheme is used, the resulting marker movement velocities violate the continuity equation for the control volume associated with the surface cell.[15]

In addition, the new simulation method incorporates new treatments for new fluid cell velocities as well as for three types of surface velocities.[15] For new fluid cell velocities the new approach is fundamentally different from previous approaches. Rather than being based on marker velocities, each new fluid cell internal velocity is assigned either the value of the closest appropriate surface or internal velocity or the average of two appropriate, equidistant surface and/or internal velocities. This new method is more efficient and requires less memory than the MAC approach and, in contrast with the SMAC approach, does not artificially introduce asymmetry.

The three types of surface velocities for which new approaches are introduced are those associated with a surface cell that has either two adjacent empty neighbours and one obstacle neighbour, two empty neighbours on opposite faces or three empty neighbours. A representative situation of a cell with one OB neighbour and two adjacent EMP neighbours is sketched in Figure 3. The situation of Figure 3 is not uncommon. It will occur repeatedly, for example, as fluid moves up the face of a vertical obstacle. The new surface velocity treatments for this and

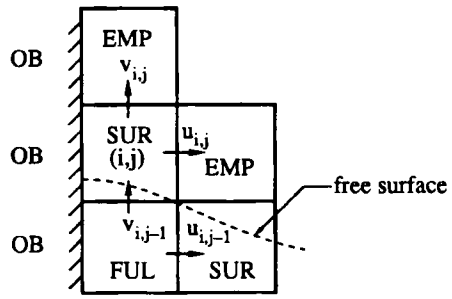

Figure 3. An SUR cell (i, j) with two adjacent EMP neighbours and one OB neighbour

similar situations have a significant effect on the simulations of flow along obstacles. For cell (i, j) of Figure 3 the new approach is to assign to the surface velocity $u_{i,j}$ either the value of $u_{i,j-1}$ if $u_{i,j-1}$ is positive or a zero value if $u_{i,j-1}$ is negative or zero. Then the other surface velocity $v_{i,j}$ is calculated to ensure that continuity is satisfied by requiring that the incompressibility deviation $D_{i,j}$ vanishes, where

$$D_{i,j} = \frac{u_{i,j} - u_{i-1,j}}{\delta x} + \frac{v_{i,j} - v_{i,j-1}}{\delta y}.$$

This new approach was adopted for the following reasons. If the MAC and SMAC assignment scheme is used for the situation shown in Figure 3, then the velocity $u_{i,j}$ is set equal to $u_{i-1,j}$, which is zero, since cell $(i-1, j)$ is an obstacle cell. As long as cell (i, j) remains a SUR cell with adjacent empty neighbours, $u_{i,j}$ remains equal to zero. This is true regardless of the value of $u_{i,j-1}$, which is the nearest fluid velocity. In this special situation the value of $u_{i-1,j}$ does not have any relation at all to the motion of the fluid that is moving up the face of the vertical obstacle. It is more appropriate, therefore, to assign to $u_{i,j}$ the value of $u_{i,j-1}$, the nearest horizontal velocity that is related to the motion of the fluid, except when $u_{i,j-1}$ is negative. If $u_{i,j}$ were assigned a negative value, the subsequent determination of $v_{i,j}$ by use of the continuity equation would lead to a value of $v_{i,j}$ that is larger than $v_{i,j-1}$ and the result would be that a very thin strip of fluid, narrower than the width of a cell, would move rapidly up the face of the obstacle. Therefore a value of zero is assigned to $u_{i,j}$ when $u_{i,j-1}$ is negative.

For a surface cell with two empty neighbours on opposite faces the new approach is to adjust the surface velocities by equal and opposite amounts, which ensures that the incompressibility deviation vanishes. Consider, for example, the case of a cell (i, j) which has empty neighbours on its right and left faces. As a result of the changes that have occurred in the values of $v_{i,j}$ and $v_{i,j-1}$ just prior to the assignment of the surface velocities $u_{i,j}$ and $u_{i-1,j}$, the incompressibility deviation $D_{i,j}$ will not in general be equal to zero. The new approach is to adjust the surface velocities according to

$$u_{i,j} = u_{i,j} - \tfrac{1}{2}D_{i,j}\delta x, \qquad u_{i-1,j} = u_{i-1,j} + \tfrac{1}{2}D_{i,j}\delta x,$$

with the result that the incompressibility deviation is zero following the assignment of surface velocities.

Finally, for a surface cell with three empty neighbours a new approach is introduced if the cell also is a new fluid cell. Assume that a small amount of fluid has just entered cell (i, j) from below. Since the pressures in the empty cells on the left and right of cell (i, j) are equal, the new

surface velocities $u_{i,j}$ and $u_{i-1,j}$ are set equal to each other and to the average of the nearest internal velocities according to

$$u_{i,j} = u_{i-1,j} = (u_{i,j-1} + u_{i-1,j-1})/2.$$

The third new surface velocity $v_{i,j}$ is simply assigned the value of the internal velocity $v_{i,j-1}$. With these choices the incompressibility deviation $D_{i,j}$ vanishes. If cell (i, j) is not a new fluid cell, the same procedure as used in the MAC method is employed, namely $u_{i,j}$ and $u_{i-1,j}$ do not change and $v_{i,j}$ is assigned the value of $v_{i,j-1}$.

The free surface pressure boundary conditions are applied at the centres of the surface cells, just as is the case in both the MAC and SMAC methods. In 1970 Chan and Street[16] introduced the Stanford University modified MAC code (SUMMAC). They introduced an 'irregular stars' scheme in order to allow the free surface pressure boundary conditions to be applied at points nearer the free surface rather than simply at the centres of the surface cells. Chan and Street showed that SUMMAC can be applied to simulate the motion of a 'solitary wave' and produces results that are superior to those obtained by use of the MAC method. In order to determine the leg lengths of an irregular star, the intersections of line segments connecting markers on the free surface and lines connecting cell centres must be determined. Hirt and Nichols[17] pointed out that the use of line segments in connection with problems in which free surfaces 'fold over' or collide leads to difficult problems that apparently have not been resolved. The approach developed by Chan and Street for the improved application of the free surface boundary condition is clearly an improvement over simply applying the pressure boundary condition at the centre of a surface cell and can be expected to lead to improved results when it can be used. As part of the authors' ongoing research, work is under way to develop an efficient procedure for applying the free surface pressure boundary condition on or near the free surface for general free surface flow problems, including those in which free surfaces collide.

In the next four sections new procedures are introduced that are related to the flags of the cells that represent solid boundaries, to the sequence of steps in the computational cycle and the intentional treatment of impact, to the adjustment for the effects of pressure of the tentative internal velocities that are associated with surface cells and to the treatment of a new type of cell. All these new procedures play an important role in the simulation of the impact of a fluid front with a solid obstacle. Following the descriptions of the new procedures, the significance of their use is demonstrated in Section 6 by numerical simulation results for three examples. In Section 7 the validity of these new procedures is demonstrated by comparisons with experimental results.

2. BOUNDARY CELL FLAGS

In the MAC, SMAC and SM methods the cells that comprise a solid boundary or obstacle are permanently assigned a special flag. In addition, since fluid cannot cross the solid boundary, the velocity normal to the face of a boundary cell is assigned a zero value when a value is required. There are two undesirable consequences of this treatment of boundary cells. First, the flag of a cell in the computational domain that is adjacent to a solid obstacle can change suddenly from empty to full immediately after a marker enters the cell. This can occur as a result of the fact that a cell is flagged as a full cell when it has no empty neighbours. Therefore, even though fluid has barely entered the column of cells adjacent to the solid obstacle shown in Figure 4, all the cells adjacent to the obstacle are nevertheless flagged as full cells, since none of them has an empty neighbour. Second, the subsequent movement towards the obstacle of the markers that represent the free surface is incorrectly retarded. After a marker has entered a cell adjacent

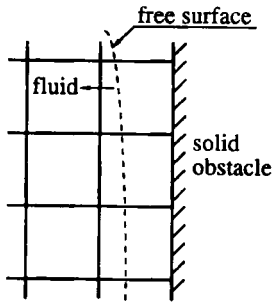

Figure 4. Free surface approaching a solid boundary

to an obstacle, the velocity normal to the face between the fluid cell and the obstacle cell becomes one of the velocities that is used to compute the velocity of the marker. Since the velocity on the obstacle cell face is assigned a value of zero, the obstacle begins to retard the advance of the marker toward the obstacle *as soon as* the fluid enters the cell adjacent to the obstacle.

In order to overcome the difficulties described above, boundary cells in the new method can be flagged either as empty cells or as obstacle cells. If initially there is no fluid in the computational cell adjacent to a particular boundary cell, both the computational cell and the boundary cell are assigned EMP flags. When a marker enters the computational cell, its flag changes from EMP to SUR, the flag of the boundary cell remains EMP and the velocity on the face shared by the computational cell and the boundary cell is treated just as any other surface velocity. This treatment continues until a marker *actually* reaches the boundary cell. When this occurs, the boundary cell flag then changes from EMP to OB and the velocity on the face shared by the two cells is then assigned a value of zero. The presence of the boundary is not felt, therefore, until the free surface actually reaches the boundary. This change in the treatment of boundary cells represents the necessary first step in the improvement of the treatment of impacts of fluid fronts with solid boundaries.

The improved treatment of impact requires, in addition to a change in the treatment of boundary cells, fundamental changes in the computational cycle of the marker-and-cell method. In the next section the SMAC computational cycle and a new computational cycle are described. The differences between the old and new computational cycles are noted and the importance of the changes to the treatment of impact is emphasized. Specific examples are presented later in the paper that provide evidence of the effects of the new treatment of boundary cells and the new computational cycle on the simulation of impacts of fluid fronts with solid boundaries.

3. COMPUTATIONAL CYCLE

The SMAC computational cycle is outlined in Figure 5, where x and y are Cartesian co-ordinates, t is the time, u and v are the x- and y-components of velocity respectively, $\tilde{u}$ and $\tilde{v}$ are the tentative velocities, ν is the kinematic viscosity, g_x and g_y are the components of the acceleration due to gravity, θ is the pseudopressure* and ψ is the pressure potential. Careful examination of Figure 5 reveals that there is no point at which impact can be adequately treated. An SMAC

* In SMAC[5] three symbols ϕ, θ and ψ are used that are related to pressure. The symbol ϕ is referred to as the 'true pressure' and is equal to the pressure divided by the density, the symbol θ is referred to as the 'pseudopressure' and ψ is simply referred to as a 'potential'. The pressure potential ψ that we refer to is precisely the potential ψ that is referred to in Reference 5.

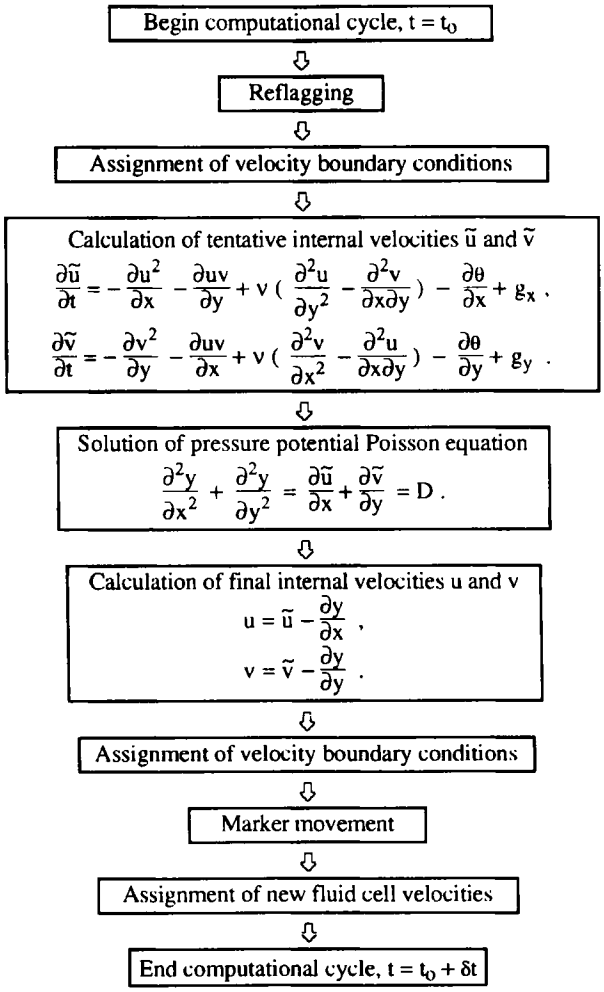

Figure 5. SMAC computational cycle

computational cycle begins at time t_0 with reflagging, the assignment of EMP, SUR and FUL flags to the cells in the computational domain based on the current distribution of markers. Next the free surface velocity boundary conditions are assigned. The free surface velocity boundary conditions consist of the surface velocities and the just outside tangential velocities. Then the tentative values of the internal velocities at time $t_0 + \delta t$ are computed from the Navier–Stokes equations with the pressure replaced by the pseudopressure θ, which is set equal to zero in the full cells.* The tentative velocities are therefore based on the internal velocity field

* In the predictor stage of the solution algorithm the pressure is replaced by an arbitrary pseudopressure θ and tentative velocities are then calculated. Since the authors of SMAC[5] state (i) that the pseudopressure field θ can *only* affect the solution efficiency of the Poisson equation, (ii) that θ *generally* is set equal to zero and (iii) that θ in some cases *must* be set equal to zero, we have decided to choose $\theta = 0$ always in full cells. A pseudopressure boundary condition is applied in surface cells to satisfy the normal stress condition.

from the previous computational cycle and the velocity boundary conditions that were assigned after reflagging in the current cycle. After the tentative velocities have been computed, the pressure potential Poisson equation is solved. By use of the calculated tentative velocities and pressure potentials, the final velocities at time $t_0 + \delta t$ are then computed. Subsequently, new values of the velocity boundary conditions are assigned. Note that the first set of velocity boundary conditions, the tentative internal velocities, the pressure potentials, the final internal velocities and the second set of velocity boundary conditions are all associated with the same distribution of markers and cell flags. The final steps in the SMAC computational cycle are the movement of markers followed by the assignment of new fluid cell internal velocities. Particular attention will be focused on the treatment of impact in this computational cycle.

Physically, impact is characterized by a sudden increase in pressure along a portion of the fluid boundary that was a part of the free surface but is now in contact with a solid obstacle. The sudden increase in pressure causes an abrupt change in the direction of fluid movement. There is no point in the SMAC computational cycle where impact can be treated properly. Assume, for example, that one or more markers representing the free surface entered a cell adjacent to an obstacle during the preceding computational cycle. This occurred as a result of the movement of markers, which was one of the last steps in that cycle. During the reflagging that occurs during the first step of the current computational cycle, the cell in question becomes an FUL cell, indicating that impact has occurred. Since the cell is now an FUL cell adjacent to a solid obstacle, the velocity on the cell face that constitutes part of the solid boundary is set equal to zero. Therefore the velocity boundary condition that is assigned immediately following reflagging also indicates that impact has occurred. Following the assignment of velocity boundary conditions, the tentative velocities $\tilde{u}$ and $\tilde{v}$ are computed. These tentative velocities are used to calculate the incompressibility deviation D, followed by the solution of the Poisson equation for the pressure potential ψ. In the previous cycle the impact cell under consideration was an EMP cell and therefore had no pressure potential associated with it at all. Since it became, after reflagging, an FUL cell adjacent to an obstacle, the pressure potential boundary condition on the cell face that constitutes part of the solid boundary now is that the gradient of the pressure potential in the direction normal to the boundary must vanish. Two problems are apparent. The first, that the cell next to the boundary becomes a full cell as soon as a marker enters it, was pointed out and resolved in the preceding section of this paper. Even when this problem is resolved, however, the second problem remains. The second problem is that there is no opportunity at any point in the SMAC computational cycle to intentionally treat the impact by taking into account the pressure pulse that occurs when the fluid impacts the obstacle. To allow the treatment of impact, the alternative computational cycle shown in Figure 6 is proposed.

The key differences between the new and old computational cycles are the relocation of the steps in which reflagging and the assignment of new fluid cell velocities occur and the use of a special pressure potential boundary condition for a cell in which impact has been identified. The first step in the new computational cycle is the movement of markers. Next the tentative internal velocities at $t_0 + \delta t$ are calculated. Note that both marker movement and the calculation of tentative velocities are based on information available at the conclusion of the previous cycle, namely on the cell flags at t_0, the internal velocity field at t_0 and the boundary velocities at t_0. In the SMAC computational cycle the tentative internal velocities are based instead on the internal velocity field at t_0 and the tentative boundary velocities assigned after reflagging. The tentative surface velocities in the new computational cycle are assigned immediately following the calculation of the tentative internal velocities. Reflagging occurs only after the determination of the complete tentative velocity field. During reflagging, impact is identified. If a marker has entered a boundary cell, the flag of the cell changes from EMP to OB and the velocity normal to the boundary face of the cell is set equal to zero. After reflagging, values are assigned for new

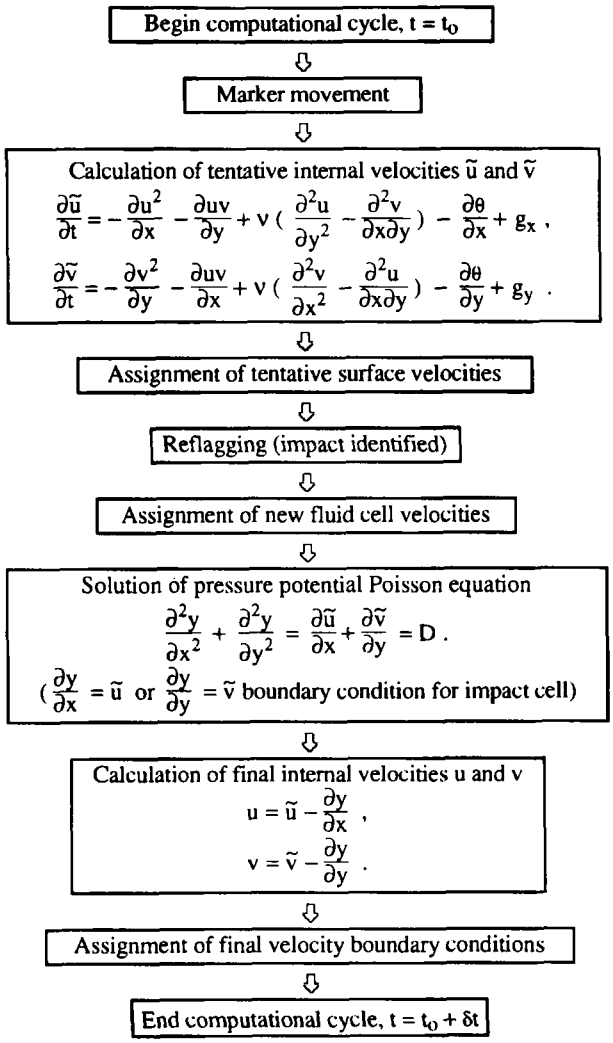

Figure 6. New computational cycle

fluid cell velocities as required. At this point the fluid configuration at $t_0 + \delta t$ is set and tentative velocities at $t_0 + \delta t$ are known. The influence of pressure on the change from the velocities at t_0 to the tentative velocities at $t_0 + \delta t$ has until this point not been computed. Now the tentative velocities $\tilde{u}$ and $\tilde{v}$ are used to compute the incompressibility deviation D and the pressure potential Poisson equation is solved. The pressure potential and tentative velocities are then used to calculate the final velocities according to

$$u = \tilde{u} - \partial\psi/\partial x, \qquad v = \tilde{v} - \partial\psi/\partial y.$$

For each cell in which impact has been identified, the velocity normal to the cell face that is coincident with the solid boundary should be reduced to zero as a result of the impact. If the

boundary is vertical, the appropriate equation for adjusting the velocity normal to the boundary for the effect of pressure is

$$u = \tilde{u} - \partial\psi/\partial x. \tag{1}$$

Therefore, if

$$\partial\psi/\partial x = \tilde{u},$$

then

$$u = 0.$$

Consequently, in the solution for ψ in the new computational cycle a new Neumann boundary condition is applied to an impact cell. In every impact cell the gradient of ψ in the direction normal to the boundary must be equal to the value of the tentative velocity normal to the boundary.

The new pressure potential boundary condition in an impact cell expresses the requirement that the gradient of the pressure potential at the boundary where the impact occurs must be such that the velocity normal to the boundary is caused to vanish as a result of the impact. This boundary condition is applied to a particular cell adjacent to a boundary only during the time step in which markers in that cell initially impact the boundary. By use of this correct boundary condition at the correct time, the large pressure pulse and gradients are correctly simulated. Following impact, the need for a special treatment no longer exists. The standard pressure boundary condition (e.g. $\partial\psi/\partial x = 0$ for a vertical boundary) applies thereafter.*

Following the solution of the pressure potential Poisson equation, the final internal velocities at $t_0 + \delta t$ are calculated. The last step is the assignment of the final surface velocities. At the end of the computational cycle the values of all relevant quantities—the marker positions, the cell flags, the internal velocities, the surface velocities and the pressure potentials—are known at time $t_0 + \delta t$.

It should be noted that one may choose to employ either pressure or pressure potential in the use of a two-stage method. If pressure is used instead of pressure potential, the Poisson equation, the impact boundary condition and the final velocity equations become

$$\frac{\partial^2 p}{\partial x^2} + \frac{\partial^2 p}{\partial y^2} = \left(\frac{\partial \tilde{u}}{\partial x} + \frac{\partial \tilde{v}}{\partial y}\right)\frac{\rho}{\delta t},$$

$$\frac{\partial p}{\partial x} = \frac{\rho \tilde{u}}{\delta t}, \qquad \frac{\partial p}{\partial y} = \frac{\rho \tilde{v}}{\delta t},$$

$$u = \tilde{u} - \frac{\partial p}{\partial x}\frac{\delta t}{\rho}, \qquad v = \tilde{v} - \frac{\partial p}{\partial y}\frac{\delta t}{\rho}.$$

No other changes are required.

4. ADJUSTMENT OF TENTATIVE VELOCITIES

The tentative internal velocities $\tilde{u}$ and $\tilde{v}$ are computed by use of the Navier–Stokes equations simplified by the elimination of the pressure terms for the full cells. In order to take into account the effect of pressure, the tentative velocities are used to calculate the incompressibility deviation

* In fact, the new impact boundary condition can actually continue to be applied after impact, since it reduces to the standard boundary condition as a result of the fact that $u = 0$ along the vertical boundary.

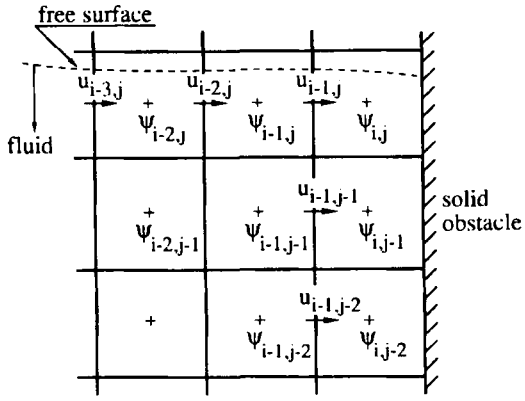

Figure 7. Adjustment of tentative velocities

D, the pressure potential Poisson equation is solved for the pressure potential ψ and the final internal velocities u and v are computed.

In the preceding sections attention has been focused on the movement of markers in cells adjacent to a solid boundary, on the flags associated with the cells that comprise a solid boundary, on the pressure potential boundary condition for a cell in which impact occurs and on the correct sequence of steps in the computational cycle for the treatment of impact. Use of the new procedures presented in the preceding sections will lead to improved estimates of the pressure potentials associated with the cells adjacent to a boundary along which impact has occurred. Use of these improved estimates of the pressure potentials will in turn lead to more appropriate adjustments of the tentative internal velocities associated with the cells adjacent to the boundary. The internal velocity associated with a surface cell in which impact has occurred requires special consideration, however.

In Figure 7 the surface cell of interest is cell (i, j) and the internal velocity $u_{i-1,j}$ is the one on which attention is focused. Since cells (i, j) and $(i-1, j)$ are both surface cells, the pressure potentials $\psi_{i,j}$ and $\psi_{i-1,j}$ are both zero. Consequently, use of the finite difference form of equation (1),

$$u_{i-1,j} = \tilde{u}_{i-1,j} - \left(\frac{\psi_{i,j} - \psi_{i-1,j}}{\delta x}\right), \tag{2}$$

to adjust the tentative internal velocity $\tilde{u}_{i-1,j}$ results in a final velocity that is identical to the tentative velocity. This result is not appropriate, since the tentative velocity $\tilde{u}_{i-1,j}$ was calculated without taking into account either the influence in general of pressure or the fact in particular that impact occurred in cell (i, j) during the current computational cycle. For cell $(i, j-1)$, on the other hand, the new procedures presented in the preceding sections of this paper lead to an estimate of $\psi_{i,j-1}$ that allows an adjustment of $\tilde{u}_{i-1,j-1}$ that does take into account the impact that occurs in cell $(i, j-1)$. A similar statement applies to cell $(i, j-2)$, pressure potential $\psi_{i,j-2}$ and tentative internal velocity $\tilde{u}_{i-1,j-2}$.

For the purpose of adjusting the tentative velocity $\tilde{u}_{i-1,j}$, we propose the use of a pressure potential gradient determined by linear extrapolation of the two closest pressure potential radients, those associated with the FUL cells $(i-1, j-1)$, $(i, j-1)$, $(i-1, j-2)$ and $(i, j-2)$

which are directly below $u_{i-1,j}$. The resulting equation for the adjustment of tentative velocity $\tilde{u}_{i-1,j}$ is

$$u_{i-1,j} = \tilde{u}_{i-1,j} - 2\left(\frac{\psi_{i,j-1} - \psi_{i-1,j-1}}{\delta x}\right) + \left(\frac{\psi_{i,j-2} - \psi_{i-1,j-2}}{\delta x}\right). \tag{3}$$

Two special cases should be noted. First, if the extrapolated pressure potential gradient has a different algebraic sign than the pressure potential gradient just below $u_{i-1,j}$, the extrapolated value is not used. The boundary condition on the free surface is that the pressure potential must vanish. A different algebraic sign would imply that the pressure potential at the free surface is non-zero. Therefore the pressure potential gradient in this case is assumed to be equal to zero and

$$u_{i-1,j} = \tilde{u}_{i-1,j}. \tag{4}$$

Second, if there is only one row of FUL cells below $u_{i-1,j}$, then the only available pressure potential gradient is that associated with the two FUL cells immediately below $u_{i-1,j}$, and the new equation used to adjust $\tilde{u}_{i-1,j}$ is

$$u_{i-1,j} = \tilde{u}_{i-1,j} - \left(\frac{\psi_{i,j-1} - \psi_{i-1,j-1}}{\delta x}\right). \tag{5}$$

Therefore the tentative velocity $\tilde{u}_{i-1,j}$ associated with a surface cell in which impact has occurred is adjusted by equation (3), (4) or (5) rather than by equation (2), the standard final velocity equation. The search for an improved treatment of impact led to the preceding new procedure for calculating the final internal velocity for a surface cell in which impact has occurred. It should be noted, however, that the tentative internal velocity on a face between any two surface cells, even if neither of them is adjacent to a boundary with which impact occurs, is also calculated without taking fully into account the influence of pressure. Furthermore, since the pressure potential in every surface cell is zero, the pressure potential gradient between any two surface cells is also zero. Therefore, when the final velocities are calculated in the standard way by use of the finite difference form of equation (1), there is actually no pressure correction of any of the tentative internal velocities, such as $\tilde{u}_{i-2,j}$ or $\tilde{u}_{i-3,j}$ of Figure 7, that are closest to the free surface. Consequently, we propose the use of the new procedure described above for the adjustment of all internal velocities that lie between surface cells, not just for an internal velocity associated with a surface cell in which impact has occurred.

5. CORNER CELL

In the preceding section new procedures for adjusting the tentative internal velocities between surface cells are presented. One situation involving impact in a surface cell requires additional attention. In the following the new term 'corner cell' refers to a surface cell that has an impact boundary on one side, a surface or full cell on the opposite side, an empty cell on one of the remaining two sides and a cell that is not a full cell (either an obstacle, empty or surface cell) on the fourth side. Cell (i, j) of Figure 8 is an example of a corner cell. The general motion of the fluid in Figure 8 is from left to right and it is assumed that impact of the advancing fluid front with the right boundary occurs during the current computational cycle. Previously, no special consideration is given to such a cell. Careful examination of the evolution of the velocities associated with corner cells reveals, however, that the treatment of corner cells has a profound effect on the numerical simulation. In what follows, a special method for the treatment of corner

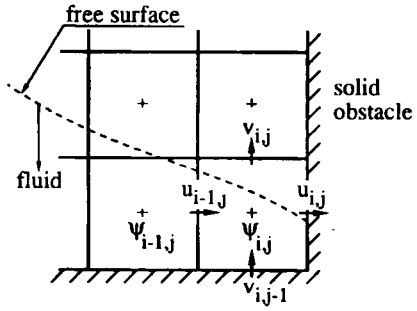

Figure 8. Impact with right boundary in corner cell (i, j)

cells is presented. Numerical examples that demonstrate the significance of the use of this new method are found in Section 6.

As a result of the movement of markers at the start of the current computational cycle, one or more markers reach the right boundary corner cell (i, j) as shown in Figure 8. Following marker movement, the tentative internal velocities, including the velocity $\tilde{u}_{i-1,j}$ on the left face of corner cell (i, j), are calculated by use of the modified Navier–Stokes equations. Even though one or more markers reached the right boundary during marker movement, the boundary cell to the right of cell (i, j) remains an EMP cell until reflagging occurs. Therefore, at the time of the assignment of tentative velocity boundary conditions, cell (i, j) is a SUR cell with two adjacent EMP neighbours. Consequently, $\tilde{u}_{i,j}$ is assigned the value of $\tilde{u}_{i-1,j}$, and $\tilde{v}_{i,j}$ is assigned the value of $\tilde{v}_{i,j-1}$, which is zero. Following the assignment of tentative velocity boundary conditions, reflagging occurs, during which the flag of cell $(i + 1, j)$ is changed from EMP to OB. The next step in the new computational cycle that involves corner cell (i, j) is the solution of the pressure potential Poisson equation. If corner cell (i, j) is treated as a regular surface cell, the pressure potential $\psi_{i,j}$ is considered a boundary condition and is set equal to zero. Consequently, there is no opportunity to impose the impact boundary condition $\partial\psi/\partial x = \tilde{u}$ on the right face of cell (i, j). The eventual result of this failure to account for impact is that the final velocity $u_{i-1,j}$ is actually larger than $\tilde{u}_{i-1,j}$. The equation for the computation of the final velocity $u_{i-1,j}$ is (recall that $\psi_{i,j} = 0$)

$$u_{i-1,j} = \tilde{u}_{i-1,j} - \left(\frac{0 - \psi_{i-1,j}}{\delta x}\right).$$

Since $\psi_{i-1,j}$ is positive, $u_{i-1,j}$ is larger than $\tilde{u}_{i-1,j}$. This result indicates that the velocity component normal to the boundary has increased as a result of the impact, instead of decreasing as expected.

In order to account for impact, a corner cell must not be treated as a regular surface cell. In the new method, instead of assigning a value of zero to $\psi_{i,j}$, the value of $\psi_{i,j}$ is computed. The required three pressure potential boundary conditions for cell (i, j) are $\partial\psi/\partial y = 0$ on the bottom face, $\partial\psi/\partial x = \tilde{u}$ on the right face and $\psi = 0$ on the top face. These boundary conditions are consistent with the facts that the normal velocity is zero on the bottom face, impact has occurred on the right face and the cell above cell (i, j) is an empty cell. By virtue of the use of the impact boundary condition on the right face of corner cell (i, j), the value computed for $\psi_{i,j}$ will be larger

than that for $\psi_{i-1,j}$. As a consequence, the final velocity $u_{i-1,j}$ which is calculated by use of

$$u_{i-1,j} = \tilde{u}_{i-1,j} - \left(\frac{\psi_{i,j} - \psi_{i-1,j}}{\delta x}\right)$$

will be smaller than $\tilde{u}_{i-1,j}$. This result indicates that the impact has caused the value of $u_{i-1,j}$ to decrease as expected.

6. SIMULATION RESULTS

In this section detailed comparisons are made between SMAC and IMPAC simulation results in order to demonstrate the effects of the new methods presented in this paper.

The IMPAC simulation method was created by extensively modifying the SM method to incorporate the new velocity boundary conditions described in Section 1 as well as the new procedures for the intentional treatment of impact presented in Sections 2–5, including the new treatment of boundary cell flags, the new computational cycle, the new pressure potential boundary condition for an impact cell, the new procedures for the adjustment of internal velocities and the new technique for the treatment of a corner cell. There is no difference between the SM and SMAC methods as far as the treatment of impact is concerned. The essential difference between the SM method itself and the SMAC method is that only a single string of markers along the free surface is used in the SM method, as opposed to the use of markers distributed throughout the fluid in the SMAC method. As a result, an SM simulation of a given problem requires less computer time and memory than an SMAC simulation of the same problem. For further discussion of the surface marker method, as well as comparisons of the simulations of several different problems by use of the SM and SMAC methods, see Reference 12.

Simulation results are presented for three different free surface fluid flow examples. Attention is focused on the velocities and pressures before and after impact in the fluid region in the neighbourhood of the impact. The computational region for each example is a 5 in × 4 in rectangle divided into 320 cells, each having dimensions of 0·25 in × 0·25 in. The kinematic viscosity of the fluid is $\nu = 1{\cdot}6 \times 10^{-3}$ in^2 s^{-1}, and the time step is $\delta t = 0{\cdot}0005$ s. A slip boundary condition is applied to flow along a solid boundary.*

6.1. First cavity-filling example

In this example a steady stream of fluid enters with a uniform velocity of 40 in s^{-1} through a gate in one side of an evacuated, two-dimensional, closed cavity that is assumed to lie in a horizontal plane. Since gravity does not affect the flow and there are no obstacles in the cavity, the expected flow pattern is plug flow until the fluid front impacts the side of the cavity opposite the gate. Of primary interest in this example is the simulation of the approach of the fluid front towards the solid boundary.

The significance of the new treatment of boundary cell flags is demonstrated in Figure 9, where two different sets of simulation results are presented. One set was obtained by use of the

* Appropriately small cells are required near solid boundaries if boundary layers are to be resolved adequately. Typically, four or five cells across the thickness of the boundary layer are necessary. Since the resolution of the boundary layer is not the primary focus of this paper, cells this small are not used. Consequently, the slip boundary condition is prescribed, since it better describes the majority of the velocity distribution in the cells adjacent to the solid boundaries. This use of a slip boundary condition does not affect any of the observations or conclusions presented.

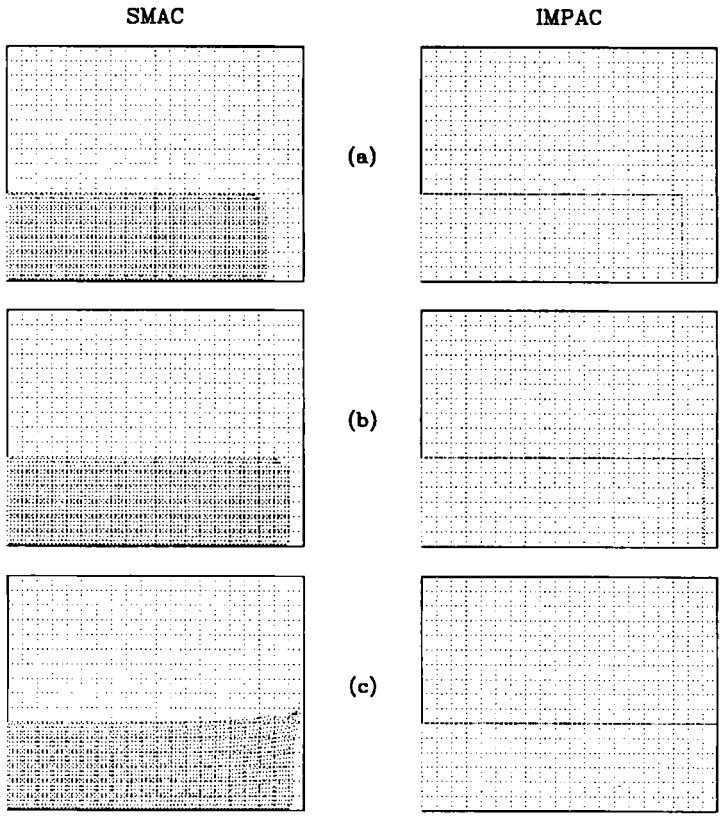

Figure 9. SMAC and IMPAC simulation results for the first cavity-filling example at (a) 0·1100 s, (b) 0·1195 s and (c) 0·1250 s

SMAC method, the other by use of the IMPAC method. In Figures 9(a)–9(c) marker plots associated with the SMAC and IMPAC simulation results are presented for times of 0·1100, 0·1195 and 0·1250 s respectively after fluid began to enter the cavity. At $t = 0{\cdot}1100$ s the fluid front has progressed across the cavity and moved through a portion of the third cell from the solid boundary. Inspection of Figure 9(a) reveals that the only discernible difference between the SMAC and IMPAC results at this time is that the advancing fluid front in the SMAC simulation has flattened corners. These flattened corners are caused by improper treatment of velocity boundary conditions, which have been corrected as demonstrated by the IMPAC results.

At $t = 0{\cdot}1195$ s the leading markers in the SMAC simulation are just about to enter the column of cells adjacent to the solid boundary. Inspection of Figure 9(b) reveals that the SMAC and IMPAC results are still the same at this time except for the flattened corners. During the next time increment, however, the leading markers in the SMAC simulation just barely enter the cells next to the solid boundary. The time increment is 0·0005 s and there is very little difference between the marker distributions at $t = 0{\cdot}1195$ and 0·1200 s. For this reason the marker plots at $t = 0{\cdot}1200$ s are not shown. There is, nevertheless, a noticeable difference between the SMAC and IMPAC results subsequent to the time that markers enter the cells adjacent to the solid boundary. Since the markers representing the free surface in the SMAC method slow down immediately after entering the cells adjacent to the boundary, the effects of the impact with the

solid boundary begin to be felt in the SMAC simulation at $t = 0{\cdot}1200$ s. For the IMPAC simulation, however, the advance of the surface markers towards the solid boundary is not affected until the surface markers *actually* reach the solid boundary.

Since the inlet speed is 40 in s^{-1} and the cavity width is 5 in, the surface markers in the IMPAC simulation reach the boundary at $t = 0{\cdot}1250$ s as shown in Figure 9(c). The SMAC simulation results displayed in Figure 9(c) clearly demonstrate that the effects of the solid boundary have been felt prior to $t = 0{\cdot}1250$ s. Close inspection of the SMAC results of Figure 9(c) reveals that the advance towards the solid boundary of the markers in the first six cells in the vertical column of cells adjacent to the boundary has been severely retarded.

The results shown in Figure 9 demonstrate the value of the new treatment of boundary cells in the simulation of the *approach* of a fluid front towards a solid boundary. The other new features presented in this paper are related to the treatment of the *impact* of the fluid front with a solid boundary. It is not enough to change the flagging scheme; one must deal with the physics of impact and make sure that the finite difference approximation is consistent with the physical phenomenon itself, which is the central focus of this work. The examples that follow demonstrate the advantages of the new treatment of impact.

6.2. Second cavity-filling example

The second example is identical to the first one except that the simple straight line front is replaced with an inclined front. An overview of the second example is presented in Figure 10, which contains marker plots of the SMAC and IMPAC simulations initially (at an arbitrarily selected position), just before impact and a short time after impact. The initial marker distribution patterns for the two simulations are shown in Figure 10(a). The just before impact marker distribution patterns are shown in Figure 10(b). In the SMAC method, as shown in the first example, the presence of the boundary is felt as soon as a marker enters the cell adjacent to the boundary. In the IMPAC solution the presence of the boundary is not felt until the free surface actually reaches the boundary. The important consequences of the treatment of impact are evidenced in Figure 10(c) by the significant differences between the two simulations that are apparent even a short time after impact. The value of the gravitational constant is zero and the initial velocity field is uniform in order to isolate the effects of impact on the velocity and pressure fields. Consequently, neither gravity nor viscosity has any influence on the flow prior to impact. The first example was chosen to highlight the importance of the new treatment of boundary cell flags on the approach of the fluid towards the boundary, while this example is intended to focus attention on the importance of the new computational cycle, impact pressure boundary conditions and corner cell treatment.

In general, the impact of an actual curved fluid front will occur initially in a small region, rather than simultaneously along a large section of the boundary as in the first example. The inclined front is a simple shape which enables the concise demonstration of a typical flow situation that involves a corner cell.* In a simulation the corner cell situation can occur regardless of the chosen computational discretization. The results that follow demonstrate that the treatment of a corner cell has a significant influence on the transient solution. Impact causes

* In Section 5 the situation involving impact in a corner cell is given special attention. While Figure 8 depicted a cell that actually occupied a corner of the computational domain, the corner cell situation may occur in any cell adjacent to a solid boundary. During any impact of a fluid front with a solid boundary, impact will occur in at least one surface cell. Such an impact surface cell is a corner cell if neither of the neighbour cells that share its faces that are normal to its impact surface is a full cell. Since there is no way to avoid this situation by a judicious choice of computation discretization, it must be dealt with.

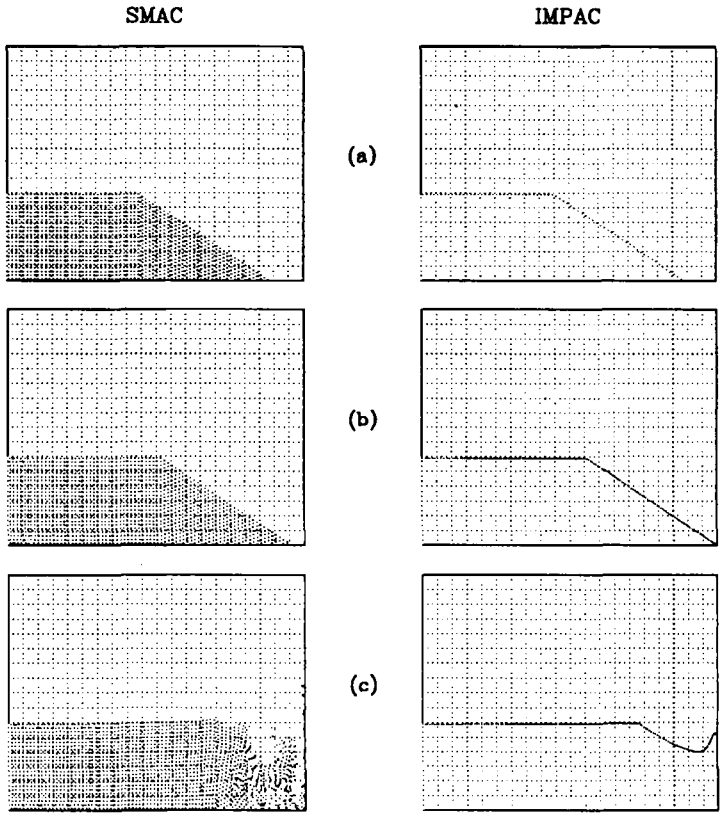

Figure 10. SMAC and IMPAC simulation results for the first cavity-filling example at (a) 0·1100 s, (b) 0·1195 s and (c) 0·1250 s

immediate and significant changes in the velocity and pressure fields in the region of impact, although it does not cause changes that are as immediate and dramatic in the positions of markers. However, since the pressures influence the velocities, which in turn determine the movement of markers, and since the markers define the extent of the computational domain, including the shape and location of the free surface, these immediate and significant changes in the velocity and pressure fields have a determining effect on the progress of the transient solution, both qualitatively and quantitatively. Therefore in this example detailed comparisons are made between the SMAC and IMPAC simulations by comparing the pressure and velocity fields in the impact region just after the occurrence of impact.

The velocities just after impact in a few of the cells in the neighbourhood of the impact are shown in Figure 11 for the SMAC and IMPAC simulations. The most striking differences between the SMAC and IMPAC results are associated with the velocity components $u_{20,2}$, $v_{20,2}$, $v_{20,3}$ and $v_{21,2}$. The values just after impact of $u_{20,2}$ and $v_{21,2}$ are both 42·4 in s^{-1} in the SMAC simulation, while they are both only 17·9 in s^{-1} in the IMPAC simulation. The vertical velocity component $v_{20,2}$ has a negative value of $-2{\cdot}4$ in s^{-1} in the SMAC results, while it has a positive value of 13·8 in s^{-1} in the IMPAC results. In the IMPAC results the value of $v_{20,3}$ also is 13·8 in s^{-1}, whereas in the SMAC results, no value is even computed for $v_{20,3}$, since cell (20, 3) is an empty cell. The new treatment of impact clearly has a dramatic effect on the changes caused by impact in the values of the velocities in the neighbourhood of the impact.

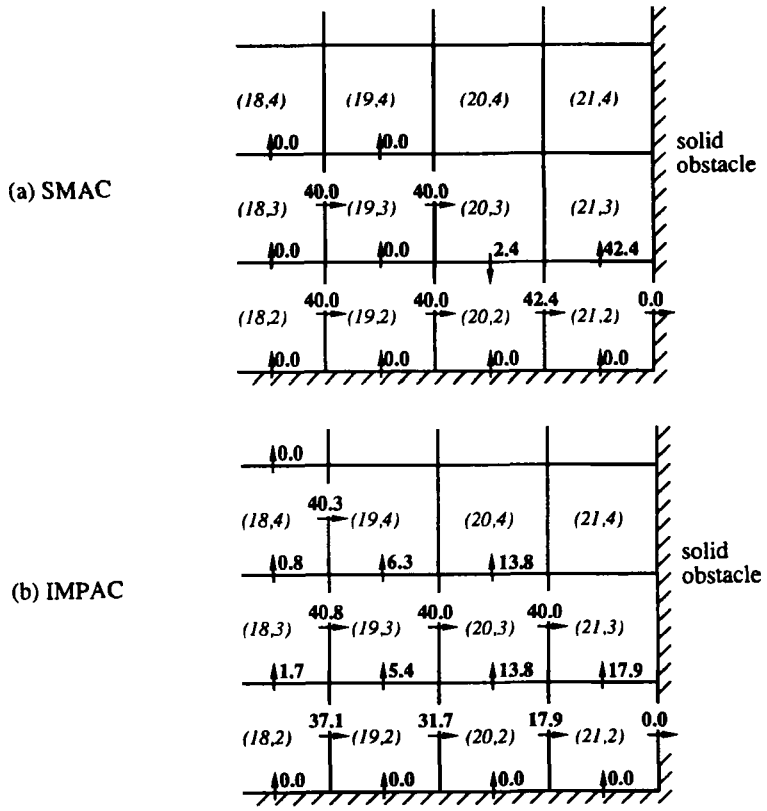

Figure 11. Second cavity-filling example results just *after* impact for $u_{i,j}$ and $v_{i,j}$ ($i = 18, 19, 20, 21$; $j = 2, 3, 4$) in in s^{-1} by use of (a) SMAC and (b) IMPAC

As shown in Figure 12, there are also very substantial differences just after impact between the IMPAC results for the pressure potential and those of the SMAC method.* For the IMPAC method the new treatment of impact allows the calculation in the corner cell (21, 2) of the large positive value of the pressure potential that is a consequence of impact, whereas the pressure potential is actually assigned a zero value in cell (21, 2) in the SMAC method. In addition, significant IMPAC pressure potential values are computed in all four of the cells displayed along the lower boundary and the gradient of the pressure potential is positive in the x-direction. In contrast, there are no non-zero pressure potential values just after impact in the SMAC results.

To properly take impact into account, it is necessary to revise the computational cycle itself and, in addition, to identify and satisfy the appropriate impact pressure boundary conditions. The IMPAC results demonstrate the benefits of implementing these modifications. For the IMPAC results the pressure in the neighbourhood of impact rises significantly and the pressure gradient towards the impact wall is positive. As a consequence, the pressure correction of the tentative velocity field to obtain the final velocity field is significant and the final velocity field

* No value of ψ is shown in an empty cell, a value of 0. is shown in a surface cell and calculated values are shown with two decimal places.

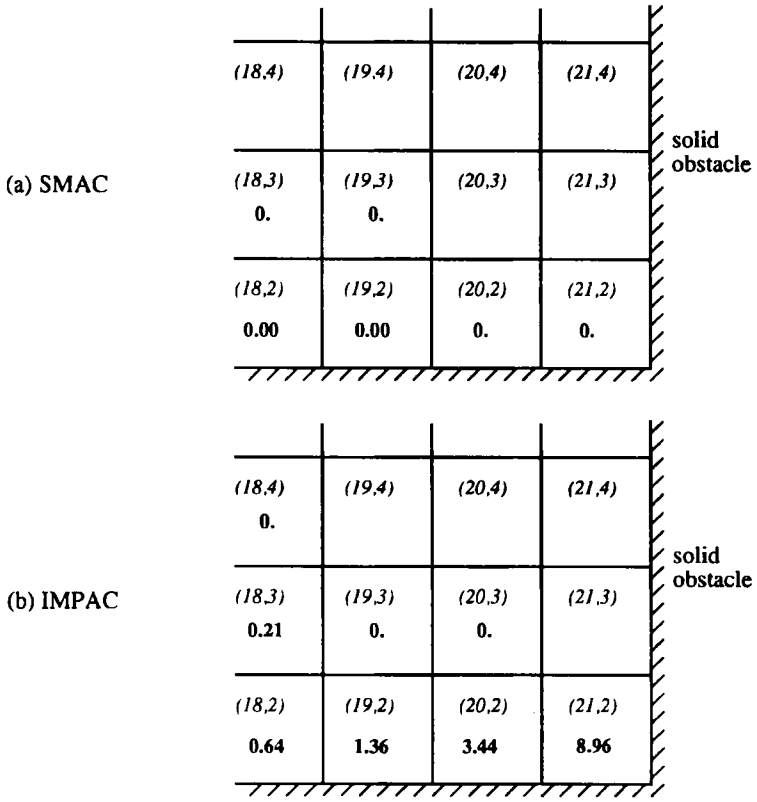

Figure 12. Second cavity-filling example results just *after* impact for $\psi_{i,j}$ ($i = 18, 19, 20, 21$; $j = 2, 3, 4$) in $\text{in}^2\ \text{s}^{-1}$ by use of (a) SMAC and (b) IMPAC

therefore differs significantly from the tentative velocity field. For example, the details of the final velocity computations for the just after impact values of $u_{20,2}$ and $v_{20,2}$ are

$$u_{20,2} = \tilde{u}_{20,2} - (\psi_{21,2} - \psi_{20,2})/\delta x = 40 - (8{\cdot}96 - 3{\cdot}44)/0{\cdot}25 = 17{\cdot}92 \text{ in s}^{-1},$$

$$v_{20,2} = \tilde{v}_{20,2} - (\psi_{20,3} - \psi_{20,2})/\delta y = 0 - (0 - 3{\cdot}44)/0{\cdot}25 = 13{\cdot}76 \text{ in s}^{-1}.$$

These drastic differences in the pressure and velocity fields in the neighbourhood of impact between SMAC on one hand and IMPAC on the other hand lead to significant differences in the progress of the transient solution, which are noticeable even a short time after impact as can be seen in Figure 10(c). The correct handling of impact in the IMPAC simulation provides for a normal redirection of the flow. The SMAC treatment of impact leads, shortly after impact, to negative pressures, negative pressure gradients in the flow direction and sustained negative transverse velocities, which result in the erratic flow pattern displayed in Figure 10(c).

6.3. *Gravity flow example*

The third example problem is the broken dam problem, in which a rectangular region of fluid initially at rest is allowed to flow down and to the right until it reaches a solid vertical boundary. The acceleration due to gravity is 386 in s^{-2}. In Figures 13(a)–13(c) marker plots are displayed

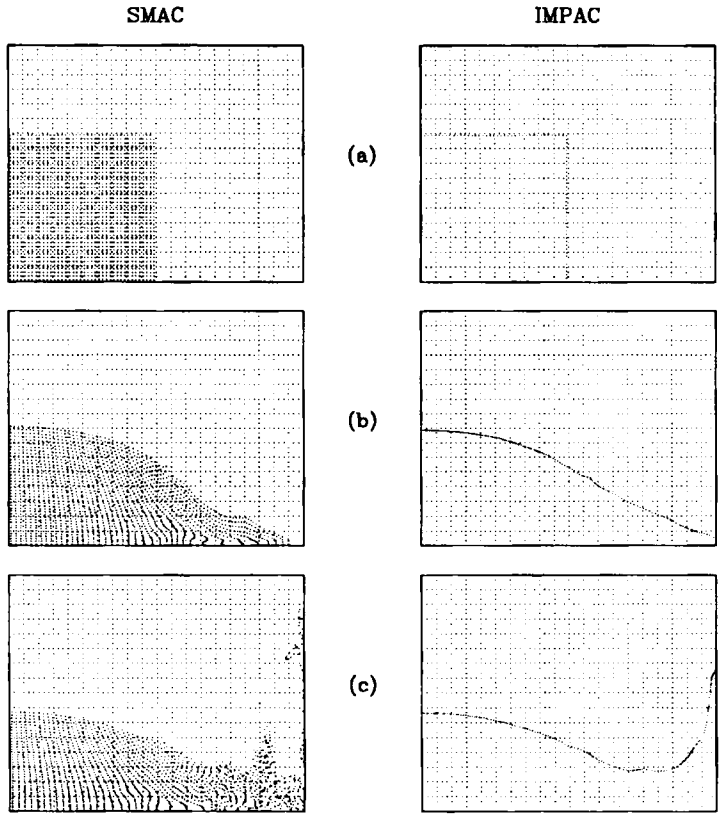

Figure 13. SMAC and IMPAC simulation results for the broken dam example (a) at 0·0 s, (b) just before impact and (c) 0·1300 s

for the SMAC and IMPAC results at $t = 0{\cdot}0$ s, just before impact and at $t = 0{\cdot}1300$ s respectively. Just before impact the leading markers in the SMAC results are just about to enter the cell adjacent to the solid vertical boundary on the right. The effects of the impact begin to be felt in the SMAC simulation immediately after markers enter the cell adjacent to the boundary, whereas in the IMPAC simulation the effects of the impact are not felt until markers actually reach the boundary.

The differences between the SMAC and IMPAC results at $t = 0{\cdot}1300$ s, just a short time after impact, are very pronounced. In the SMAC solution there is a finger of markers protruding to the left approximately three-quarters of the way up the narrow, sparse column of markers that is adjacent to the right boundary; there is a second shorter, wider column of markers that peaks in the third column of cells from the right boundary; and there is a large area to the right of this second column that is void of markers. None of these features is found in the IMPAC simulation.

The IMPAC simulation results have been compared with the SMAC results in order to isolate the effects of the new methods for the treatment of impact and demonstrate their significance. In the next section the validity of the new method is demonstrated by comparisons of simulation and experimental results.

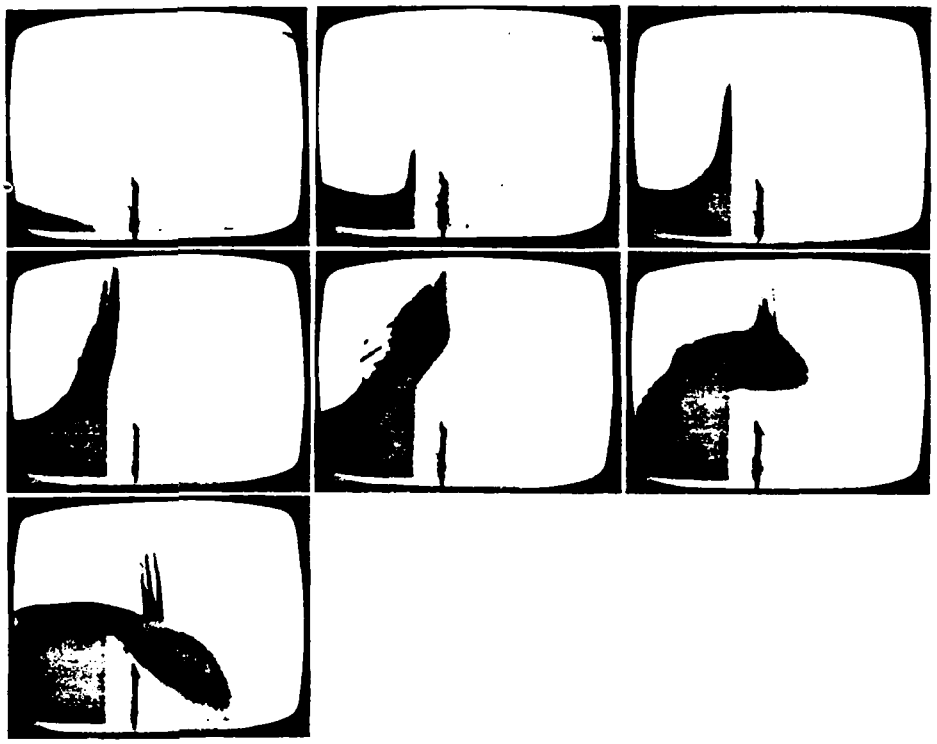

Figure 14. Experimental results of Greenspan and Young for flow over a containment dike

7. VALIDATION

Greenspan and Young[13] videotaped the flow of water that is suddenly released from a container, flows under the influence of gravity along a channel and finally impacts a vertical dike that extends across the channel. Figure 14 is a facsimile of one of the original plates of photographs that appeared as Figure 8 in Greenspan and Young's paper and was kindly provided to us by Professor Greenspan. The symbols H and R correspond to the height and width of the container respectively, L represents the distance between the container and the dike and a denotes the height of the dike. A corresponding sequence of IMPAC simulation results is shown in Figure 15. The same values of H, L, R and a are associated with the experiment of Figure 14 and the simulation of Figure 15. Inspection of these figures leads one to conclude that the simulation results bear a striking similarity to the experimental results even for this transient problem that involves impact and rapidly changing free surfaces. One of the questions of interest to Greenspan and Young was 'What percentage of the water spills over the dike after a sudden rupture of the container?'. The answers obtained experimentally and by use of our simulation are essentially the same; by either method, approximately 20% of the water spills over the dike.

8. CONCLUSIONS

Impacts of advancing fluid fronts with solid obstacles are common occurrences. At points in time and space that are close to the time and location of such impacts, relatively rapid changes

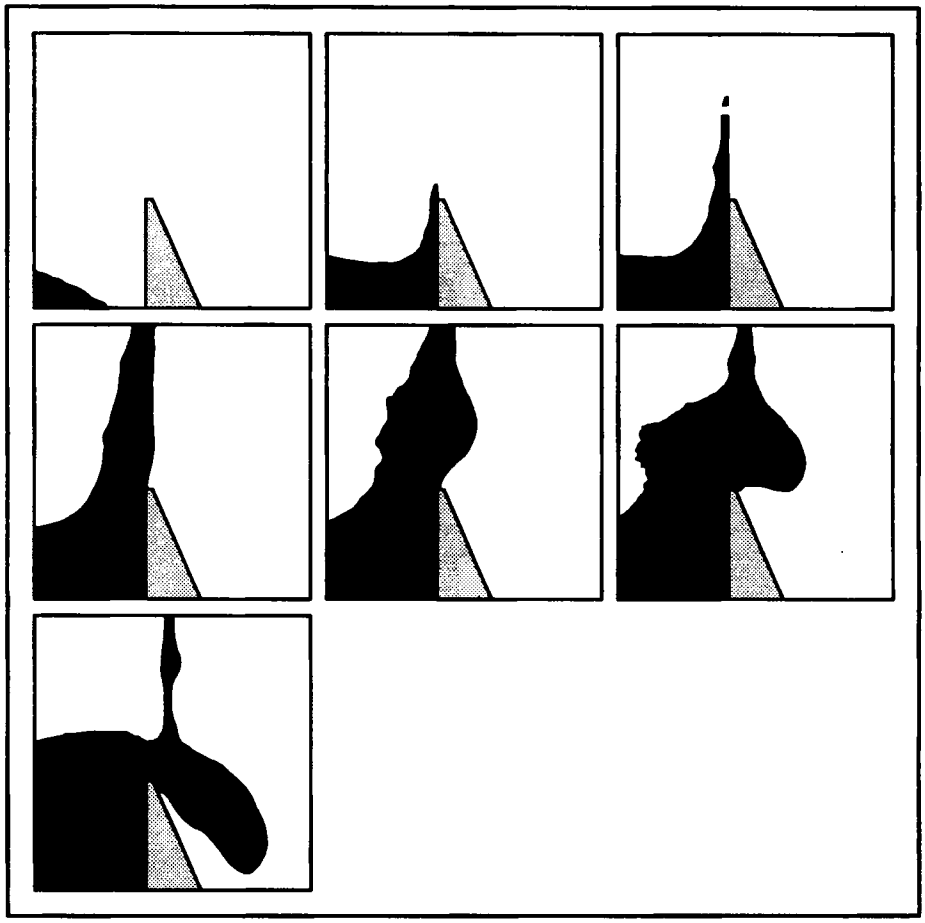

Figure 15. Modified IMPAC simulation results for flow over a dike (plots correspond to the sequence of photographs shown in Figure 14)

occur in both pressure and velocity. Therefore it is not surprising that special care must be taken in the simulation of impact. Deficiencies in the simulation of impacts of fluid free surfaces with solid boundaries by use of previous marker-and-cell methods are revealed by careful examination of the details of the methods as well as of simulation results for specific problems. New procedures that overcome these deficiencies and allow the intentional treatment of impact are presented. Some of the new procedures, such as the revised computational cycle, represent fundamental changes in the marker-and-cell method, whereas others, such as the treatment of a corner cell, represent special procedures for the treatment of specific situations that occur in connection with impact. Simulation results are presented for two cavity-filling examples and a gravity flow example. The results clearly demonstrate both the deficiencies in previous methods and the advantages of the new procedures for the treatment of impact. Finally, the validity of the new procedures is demonstrated by comparison of simulation and experimental results for a very complex free surface flow problem that involves a body of fluid impacting and subsequently overflowing a containment dike.

ACKNOWLEDGEMENTS

Support for this research has been provided by the Defense Advanced Research Project Agency of the U.S. Department of Defense as Projects 5-25084 and 5-25085 of Contract MDA093-86-C-0182, the National Science Foundation under grant DDM-9114846, and the Leadwell CNC Machines Manufacturing Corporation.

REFERENCES

1. F. H. Harlow and J. E. Welch, 'Numerical calculation of time-dependent viscous incompressible flow of fluid with free surface', *Phys. Fluids*, **8**, 2182–2189 (1965).
2. J. E. Welch, F. H. Harlow, J. P. Shannon and B. J. Daly, 'The MAC method: a computing technique for solving viscous, incompressible, transient fluid-flow problems involving free surfaces', *Los Alamos Scientific Laboratory Rep. LA-3425*, 1965.
3. A. J. Chorin, 'A numerical method for solving incompressible viscous flow problems', *J. Comput. Phys.*, **2**, 12–26 (1967).
4. J. A. Viecelli, 'A method for including arbitrary external boundaries in the MAC incompressible fluid computing technique', *J. Comput. Phys.*, **4**, 543–551 (1969).
5. A. A. Amsden and F. H. Harlow, 'The SMAC method: a numerical technique for calculating incompressible fluid flows', *Los Alamos Scientific Laboratory Rep. LA-4370*, 1970.
6. J. A. Viecelli, 'A computing method for incompressible flows bounded by moving walls', *J. Comput. Phys.*, **8**, 119–143 (1971).
7. C. W. Hirt and J. L. Cook, 'Calculating of three-dimensional flows around structures and over rough terrain', *J. Comput. Phys.*, **10**, 324–340 (1972).
8. C. W. Hirt, B. D. Nichols and N. C. Romero, 'SOLA—a numerical solution algorithm for transient fluid flows', *Los Alamos Scientific Laboratory Rep. LA-5852*, 1975.
9. B. D. Nichols, C. W. Hirt and R. S. Hotchkiss, 'SOLA-VOF: A solution algorithm for transient fluid flow with multiple free boundaries', *Los Alamos Scientific Laboratory Rep. LA-8355*, 1980; C. W. Hirt and B. D. Nichols, 'Volume of fluid (VOF) method for the dynamics of free boundaries', *J. Comput. Phys.*, **39**, 201–225 (1981).
10. P. M. Gresho and R. L. Sani, 'On the pressure boundary conditions for the incompressible Navier–Stokes equations', *Int. j. numer. methods fluids*, **7**, 1111–1145 (1987).
11. M. Rosenfeld, D. Kwak and M. Vinokur, 'A fractional step solution method for the unsteady incompressible Navier–Stokes equations in generalized coordinate systems', *J. Comput. Phys.*, **94**, 102–137 (1991).
12. S. Chen, D. B. Johnson and P. E. Raad, 'The surface marker method', in *Computational Modeling of Free and Moving Boundary Problems*, Vol. 1, *Fluid Flow*, de Gruyter, New York, 1991, pp. 223–234.
13. H. P. Greenspan and R. E. Young, 'Flow over a containment dyke', *J. Fluid Mech.*, **87**, 179–192 (1978).
14. J. P. Dear and J. E. Field, 'High-speed photography of surface geometry effects in liquid/solid impact', *J. Appl. Phys.*, **63**, 1015–1021 (1988).
15. S. Chen, 'The SMU method: a numerical scheme for calculating incompressible free surface fluid flows by the surface marker utility', *Ph.D. Dissertation*, Southern Methodist University, Dallas, TX, 1991.
16. R. K.-C. Chan and R. L. Street, 'A computer study of finite-amplitude water waves', *J. Comput. Phys.*, **6**, 68–94 (1970).
17. C. W. Hirt and B. D. Nichols, 'Volume of fluid (VOF) method for the dynamics of free boundaries', *J. Comput. Phys.*, **39**, 201–225 (1981).